Remaining Useful Life Prediction of Lithium-Ion Batteries via Improved Dream Optimization Algorithm-Tuned LSTM Networks

Suoxun Li, Jintao Liu, Yikang Zhao, Xiaoxue Wang*
Hebei University of Technology, 5340 Xiping Road, Beichen District, Tianjin, 300401, China
E-mail: 15632456222@163.com
*Corresponding author

Keywords: Lithium-ion battery, remaining useful life, dream optimization algorithm, long short-term memory

Received: February 3, 2026

Text of the abstract: Lithium-ion batteries have been widely utilized in modern society due to their excellent performance, making the accurate prediction of their remaining useful life (RUL) of paramount importance. Current RUL prediction methods are primarily categorized into battery discharge model-based approaches and data-driven approaches. However, the charging and discharging processes of batteries are typically accompanied by nonlinear variations in internal structural parameters, which pose significant challenges for model-based prediction methods. To address this issue, this paper proposes a predictive model based on Long Short-Term Memory (LSTM) networks optimized by an Improved Dream Optimization Algorithm (IDOA). First, to overcome the limitations of the original Dream Optimization Algorithm (DOA)—namely, the tendencies to become trapped in local optima and slow convergence—an optimal point set is employed for population initialization, and an adaptive population reduction mechanism is introduced to accelerate convergence. Second, the IDOA is utilized to optimize the hyperparameters of the LSTM network, thereby enhancing its predictive capability. Finally, simulation experiments are conducted using the CALCE and NASA battery datasets via the leave-one-out cross-validation method. The performance is evaluated using the average Root Mean Square Error (RMSE) and Mean Absolute Error (MAE) calculated over ten independent runs. Comparative analysis with the original DOA and other baseline models demonstrates that the proposed IDOA-LSTM model can accurately predict the RUL of lithium-ion batteries with higher precision. Specifically, for the four batteries in the CALCE dataset, the RMSE values are 0.0201, 0.0198, 0.0213, and 0.0186, while the MAE values are 0.0181, 0.0174, 0.0163, and 0.0154, respectively. The results indicate that the average prediction accuracy of the proposed model is improved by 53.8% compared to the unoptimized model.

Povzetek: Raziskava predstavlja izboljšan model IDOA-LSTM, ki natančneje napoveduje preostalo življenjsko dobo litij-ionskih baterij.

1 Introduction

In recent years, lithium-ion batteries have assumed a crucial role in addressing energy and environmental challenges. Compared to other battery types, lithium-ion batteries exhibit high power density and extended endurance. However, these batteries frequently undergo a permanent decline in performance and capacity [1] during the charging and discharging cycles. Consequently, accurately predicting the remaining useful life (RUL) of lithium-ion batteries is of significant practical importance for ensuring their safe and stable operation [2].

Recent advancements in data-driven and machine learning technologies have led to the classification of remaining useful life (RUL) prediction methods for lithium batteries into two primary categories: data-driven prediction methods and battery discharge model-based prediction methods [3]. Model-based prediction methods investigate the internal mechanisms of battery discharge to establish a chemical model that elucidates the degradation processes of the battery. This approach offers the advantage of accurately representing the complex chemical reactions occurring within the battery, thereby achieving relatively high prediction accuracy. However, a notable disadvantage is that the internal parameters of the battery continuously change as the reactions progress, necessitating ongoing measurements of the required conditions to maintain prediction accuracy. Guo [4] et al. employed a Transformer model constrained by physical information to predict the RUL of lithium-ion batteries, effectively integrating the discharge model with machine learning techniques and yielding favorable prediction outcomes. Li [5] et al. utilized electrochemical impedance spectroscopy data in conjunction with convolutional neural networks to forecast the remaining life of lithium-ion batteries, allowing for a more direct reflection of the internal mechanisms of the battery.

In contrast, prediction methods based on data-driven and machine learning can automatically extract relevant features and ignore the intrinsic relationships among various physical quantities. Common methods include support vector machine [6] (SVM). recurrent neural network [7] (RNN), long short-term memory network [8] (LSTM), etc. The accuracy of data-driven prediction methods depends on the quality and quantity of the established data samples. Its drawback is that the prediction process is not visualized and requires repeated training to achieve good prediction results. Related works summary is shown in Table 1.

Table 1: Summary on related works

Ref	Year	Objective	Dataset	Performance Metrics	Key Findings
9	2025	Proposes an AttentiveLSTM model to simultaneously and accurately predict lithium-ion battery SOH and RUL.	NASA dataset for training and the Oxford dataset for validation.	Evaluates predictive performance using R^2, MAPE, MSE, RMSE, and RE.	The model significantly outperforms existing baselines in prediction accuracy, convergence speed, and noise robustness.
10	2023	Proposes a MOAOA-DELM hybrid model for accurate and stable battery RUL prediction.	Uses the NASA lithium-ion battery aging dataset.	Evaluates predictive performance using MAE, RMSE, MAPE, RA, TIC, and IA.	MOAOA-DELM significantly outperforms existing models in accuracy and robustness.
11	2023	Proposes a GPGM hybrid model for accurate battery RUL prediction.	Uses the NASA battery aging dataset.	Evaluates using Root Mean Squared Error (RMSE), Error Rate (ER), and Explained Variance Score (EVS).	The model outperforms other methods in both one-step and multi-step prediction accuracy, requiring only limited historical data.
12	2025	Proposes a hybrid data-driven granular model for interval-based battery RUL prediction.	Uses an open-access dataset of 124 commercial lithium-ion batteries.	Evaluates performance using RMSE, MAE, Coverage (Cov), Specificity (Sp), and Quality (Q).	The model significantly outperforms baseline methods in both point and interval prediction accuracy.
13	2025	Proposes a DCI-KANs architecture to enhance the accuracy and robustness of battery RUL prediction.	Uses the public NASA PCOE and CALCE lithium-ion battery datasets.	Evaluates predictive performance using MAE, RMSE, MAPE, and ARE.	The model significantly outperforms baseline methods, reducing ARE by 43% on the NASA dataset and 22% on the CALCE dataset.
14	2025	Proposes a lightweight LTM-Net for efficient and accurate battery RUL prediction.	Uses the CALCE dataset and real-world EV operation data.	Evaluates predictive performance using AE, MAE, RMSE, and RULape.	Outperforms baseline models in accuracy and speed, efficiently handling arbitrary-length inputs.
15	2024	Proposes a PF-BiGRU-TSAM data-model interactive approach combining data-driven and model-based advantages for battery RUL prediction.	Validated using the open-access NASA aging dataset of four lithium-ion batteries.	Evaluates predictive performance primarily using RUL absolute error and RUL absolute relative error.	The approach significantly outperforms baselines in prediction accuracy and effectively quantifies uncertainty by providing 95% confidence intervals.
16	2023	Proposes a TCN-GRU-DNN hybrid model with dual attention to improve battery RUL prediction accuracy.	Trained and validated using the public NASA and CALCE battery datasets.	Evaluates performance using AE, RMSE, MAE, and R-squared	The dual attention mechanism effectively captures capacity regeneration and degradation, achieving superior predictive performance.

In conclusion, this paper presents a data-driven model, IDOA-LSTM, for predicting the remaining useful life of lithium-ion batteries. The model begins by normalizing the dataset and subsequently dividing it into training and test datasets. To address the characteristics of the Dream Optimization Algorithm (DOA), including random initialization and slow convergence speed, two distinct strategies were implemented for enhancement, resulting in the Improved Dream Optimization Algorithm (IDOA). The model was trained using the training dataset, during which the IDOA was employed to optimize and identify the optimal hyperparameters for the LSTM model. Finally, the test dataset was input into the IDOA-LSTM model for RUL prediction, followed by a comprehensive analysis of the prediction evaluation indicators. The results indicate that the IDOA-LSTM model demonstrates high accuracy in predicting the RUL of lithium-ion batteries.

Specifically, this study aims to answer the following research questions:

(1) Can the proposed IDOA-tuned LSTM framework outperform existing optimization-based LSTM variants in RUL prediction across both monotonic and non-monotonic battery degradation datasets?

(2) Do the specific IDOA enhancements yield a statistically significant improvement in predictive robustness compared to the standard DOA? The intended outcome of this research is the development of a highly generalized and automated RUL prediction model. The success criteria are defined as achieving consistently lower prediction errors (RMSE and MAE) than state-of-the-art baselines, alongside demonstrating tight error variances and statistical significance ($p < 0.05$) across multiple independent runs.

2 Dataset selection and data preprocessing

2.1 CALCE lithium-ion battery dataset

The aging data for the lithium-ion batteries utilized in this study is sourced from the public dataset of CALCE. Specifically, four battery types from the CS2 series—CS2_35, CS2_36, CS2_37, and CS2_38—were selected as experimental subjects, each with a capacity of 1.1 Ah. These batteries were charged in constant current mode at a rate of 0.5 C. Charging continued in constant voltage mode once the battery voltage reached 4.2 V, until the charging current decreased to 20 mA, at which point the charging process was deemed complete. Subsequently, the batteries were discharged continuously at a constant current rate of 1 C until the voltage fell to 2.7 V. The capacities of the four battery types exhibited a declining trend as the number of cycles increased, with their variation curves presented in Figure 1. A battery is considered to have reached its end of life (EOL) when its available capacity drops to 70% of its rated capacity.

2.2 NASA PCoE

This article presents the lithium-ion battery aging dataset provided by NASA's Center of Excellence for Predictive Excellence (PCoE). Four groups of 18650 lithium cobalt oxide batteries, designated as B0005, B0006, B0007, and B0018, were selected from this dataset for further investigation, each with a rated capacity of 2.0 Ah. Given the limited sample size of NASA's battery dataset, the hyperparameters of the predictive model are critical. In contrast to the previously mentioned CALCE dataset, a distinctive characteristic of the NASA dataset is the presence of significant capacity recovery phenomena within its capacity degradation curve. The interspersed impedance testing and static resting phases during the experiment allow the electrochemically active materials within the battery to partially recover after brief periods of rest, leading to non-monotonic and pronounced fluctuations in the capacity curve. This study focuses on these four datasets to assess the optimization accuracy and capture capability of the IDOA-LSTM model when confronted with such highly nonlinear and irregularly fluctuating data, thereby providing a comprehensive evaluation of the practical engineering applicability of the predictive method. The capacity attenuation curves for the four battery groups are illustrated in Figure 1.

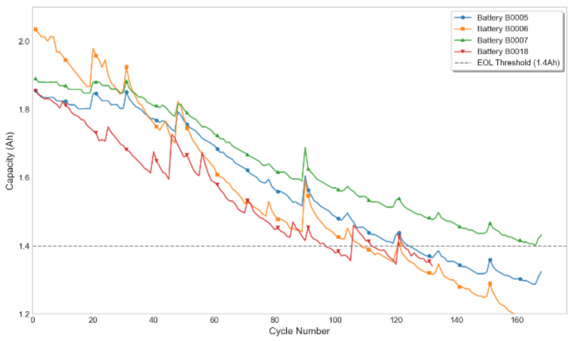

(a) CALCE battery degradation curve

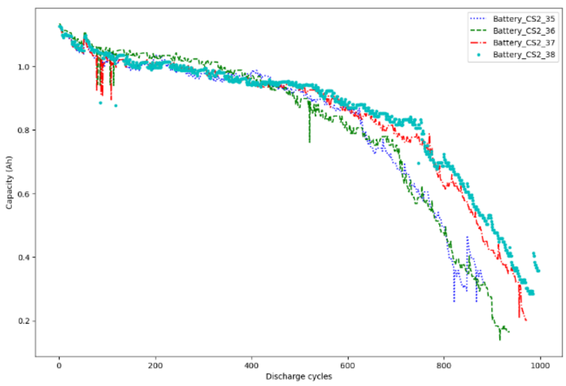

(b) NASA battery degradation curve

Figure 1: Dataset battery capacity degradation curve

2.3 Data preprocessing

(1) Hampel filter

This paper employs the Hampel filter, developed by the German mathematician and statistician Johann Hampel in 1974, as the method for data preprocessing. This technique serves as both an outlier detection method based on intermediate values and a linear filter. Given that battery capacity data is frequently affected by sensor noise during acquisition, resulting in instantaneous pulses, this study applies the Hampel filter for data cleansing. The method identifies abnormal data by calculating the median value m_i and the estimated standard deviation σ_i of the absolute deviation of the median of the sample in the window. If the data value deviates from the median by more than $3\sigma_i$, it will be replaced by the window median. This method not only retains the accuracy of the battery data, but also effectively filters the high-frequency noise.

(2) Normalization processing

Data normalization is the key link of data processing in the process of machine learning. Due to the different dimensions of input eigenvalues, it is difficult to converge in model training, which ultimately affects the prediction accuracy of the model. Normalization can realize the unification of data, improve the model to establish a stable mapping relationship, and enhance the generalization ability. At present, the commonly used normalization methods are Z-score method and Min-Max method. In this paper, the Min-Max normalization method is selected because it can effectively preserve the relative relationship between data and greatly improve the prediction accuracy of subsequent prediction models. The principle of min max method is to linearly change the original sample, map each value to a certain range, and the calculation formula is:

$$x'_M = \frac{(x - x_{\min})}{(x_{\max} - x_{\min})} \tag{1}$$

In the formula: x'_M is the normalized sample, x is the original sample, x_{min} is the minimum value in the sequence, and x_{max} is the maximum value in the sequence. This method can convert all samples in the sequence to the normal 0-1 interval, so this method can retain the relative size relationship in the original data.

3 Prediction methods

3.1 IDOA-LSTM model

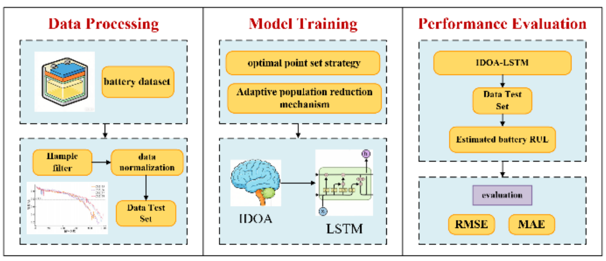

Figure 2: Flowchart of the IDOA-LSTM prediction model

The LSTM algorithm has good prediction accuracy in predicting time series data, while the DOA algorithm has a good effect in optimizing LSTM hyperparameters. Therefore, combined with the model structure mentioned above, the complete process of the lithium-ion battery RUL prediction model based on IDOA-LSTM proposed in this paper is shown in Figure 2. All the steps of this model are implemented in Python language. The steps are described as follows:

(1) The CALCE battery dataset was preprocessed. Hampel filtering was used to eliminate outliers in the dataset and normalize the data to obtain the data test set.

(2) Utilize the improved dream optimization algorithm to optimize the hyperparameters of LSTM (initial learning rate, regularization coefficient, and the number of cells in the hidden layer).

(3) Utilize the optimized LSTM prediction model to predict the data test set, obtain the estimation of the remaining battery life curve, and evaluate the prediction results using the root mean square error and the mean absolute error.

3.2 LSTM long short-term memory model

LSTM is a neural network model that enhances the traditional RNN framework. In addition to preserving the layer transfer relationships between preceding and subsequent time steps inherent in the RNN architecture, LSTM networks incorporate correlation information between the cell states of these time steps. Specifically, the neurons within an LSTM network analyse three input variables concurrently. The structure of LSTM is illustrated in Figure 3.

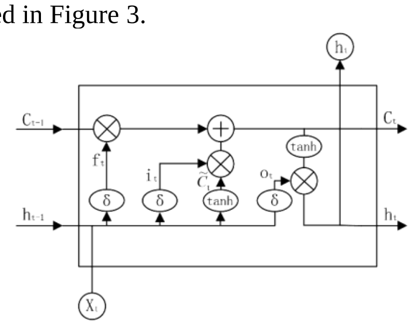

Figure 3: LSTM unit structure

3.3 Structure of the LSTM model

(1) Forgetting Gate: The primary function of the forget gate is to selectively discard irrelevant or obsolete information from the cell state. When the result of the forgetting gate approaches 0, it is easier to forget. The closer the result is to 1, the lower the chance of being forgotten. The forgetting gate can choose to retain the information in the model and discard the information in the model, which is the role that the forgetting gate plays in the model.

(2) Input Gate: In neural networks, the primary function of an input gate is to perform feature screening on the input data, including the current unit state value of the input gate. Here, C_t represents the current cell status value of the input gate. After the information is filtered through the forgetting gate, it enters the input gate. Which parameters need to be updated is determined by the input gate.

(3) Output Gate: The main function of an output gate is to transfer information. Moreover, the closer its output result is to 0, the smaller the impact of the current state on the final result. The closer its output result is to 1, the greater the impact of the current state on the final result, where O_t is the output value of this unit.

At time c, the input of LSTM is the X_t sequence, the state of the hidden layer at time u is t-1, and the state of the memory unit at time u is h_{t-1}. Through the calculation of the activation function t-1, it can be obtained that:

$$f_t = \delta(W_f[h_{t-1}, x_t] + b_f) \tag{2}$$

$$i_t = \delta(W_i[h_{t-1}, x_t] + b_i) \tag{3}$$

$$o_t = \delta(W_o[h_{t-1}, x_t] + b_o) \tag{4}$$

In the formula: f_t, i_t, and o_t respectively represent the calculation results of the forget gate, input gate, and output gate; W_f, W_i, and W_o are the weight matrices of the three. b_f, b_i, and b_o are the bias terms of the three. After the t moment, C_t and the hidden layer state h_t are represented as:

$$\tilde{C} = \tanh(W_c[h_{t-1}, x_t] + b_c) \tag{5}$$

$$C_t = f_t \odot C_{t-1} + i_t \odot \tilde{C} \tag{6}$$

$$h_t = o_t \cdot \tanh(C_t) \tag{7}$$

In the formula: $\tilde{C}$ is the candidate state update value; W_c and b_c are respectively the updated weight matrix and the bias term; The symbol $\odot$ indicates multiplication by element.

3.4 Dream Optimization Algorithm (DOA)

The Dream Optimization Algorithm [17] is an optimization technique inspired by three distinct behaviours observed in human dreams. Its fundamental framework comprises three components: memory retention, partial forgetting, and self-organizing behaviour. The subsequent sections will provide a detailed overview of the Dream Optimization Algorithm.

(1) Population initialization

Similar to other algorithms, in the initialization stage, DOA first generates a random population in the search space as the initial population, thereby initiating the optimization process of the algorithm. The initial equation of the population is as follows:

$$X_i = rand \times (X_u - X_l), i = 1, 2, ..., N \tag{8}$$

Here, N represents the number of individuals, that is, the size of the group; X_i is the i-th individual in the group; X_j and X_u respectively represent the lower and upper boundaries of the search space; $rand$ is a Dim-dimensional vector, with each dimension being a random number between 0 and 1. The obtained group can be represented as follows:

$$X = \begin{bmatrix} X_1 \\ X_2 \\ \vdots \\ X_i \\ \vdots \\ X_N \end{bmatrix} = \begin{bmatrix} X_{1,1} & X_{1,2} & \cdots & X_{1,j} & \cdots & X_{1,Dim} \\ X_{2,1} & X_{2,2} & \cdots & X_{2,j} & \cdots & X_{2,Dim} \\ \vdots & \vdots & \vdots & \vdots & \vdots & \vdots \\ X_{i,1} & X_{i,2} & \cdots & X_{i,j} & \cdots & X_{i,Dim} \\ \vdots & \vdots & \vdots & \vdots & \vdots & \vdots \\ X_{N,1} & X_{N,2} & \cdots & X_{N,j} & \cdots & X_{N,Dim} \end{bmatrix} \tag{9}$$

(2) Population exploration stage

In the exploration stage (iteration count from 0 to T_d), the population is first divided into 5 groups based on the difference in memory ability. Each iteration is regarded as a dream-making behaviour. By continuously executing the dream-making behaviour, the algorithm seeks the optimal solution for the population. Before each dream, all individuals in each group were shown the best dreams they had had before.

$$X_i^{t+1} = X_{bestq}^t \tag{10}$$

Here, X_i^{t+1} represents the $t+1$-th individual during iteration i, and X_{bestq}^t represents the best individual in group t during iteration q.

Because individuals randomly forget some information (referred to as the forgetting dimension), only the positions within the forgetting dimension are updated. The different memory capabilities of the population imply different dimensions of forgetting, which are represented by parameters K_1, K_2, K_3, K_4, K_5. This process is called the forgetting and supplementing strategy, and the formula is as follows:

$$x_{i,j}^{t+1} = x_{bestq,j}^t + (x_{l,j} + rand \times (x_{u,j} - x_{l,j})) \times \frac{1}{2} \times (\cos(\pi \times \frac{t + T_{\max} - T_d}{T_{\max}} + 1)), j = K_1, K_2, ..., K_{k_q} \tag{11}$$

Here, $X_{i,j}^{t+1}$ represents the position of the $t+1$-th individual in the j-th dimension when iterating; $X_{bestq,j}^t$ indicates the position of the best individual in group t in the q dimension during iteration j. $X_{l,j}$ and $X_{u,j}$ are respectively the lower and upper bounds of the search space in the j dimension. $rand$ is a random number between 0 and 1; t represents the current number of iterations, $T_{\max}$ represents the maximum number of iterations, and T_d represents the maximum number of iterations during the exploration phase.

First, reset the position of each individual to the position of the best individual in its group from the previous iteration. Then, randomly select the Dim dimension from the K_q dimension and represent it as K_1, K_2, ..., K_q, and update the positions in these dimensions, where q = 1,2,3,4,5 represent the group numbers. In each iteration, updates are made successively from the 1st individual to the N individual. Meanwhile, the dream sharing strategy in DOA enhances the ability to evade local optima. This strategy operates in parallel with the forgetting and supplementation strategies and follows the memory strategy, allowing individuals to randomly obtain the location information of other individuals in the forgetting dimension. The update formula is as follows:

$$x_{i,j}^{t+1} = \begin{cases} x_{m,j}^{t+1}, m \le i \\ x_{i,j}^{t}, i \le m \le N \end{cases} \tag{12}$$

Here, $x_{i,j}^{t+1}$ represents the position of the *t+1*-th individual in the i-th dimension when iterating *j*; *m* is a natural number randomly selected from the range [1, *N*] for each dimension update.

(3) Population exploitation stage

During the mining phase, before each dream-making phase, the best dream is selected from the previous iterations of the entire population and presented to the population. Update the position of each individual in the forgotten dimension. All individuals in the population have the same number of forgotten dimensions, denoted as K_r. Select *D* forgotten dimensions from k_r dimensions, denoted as K_1, K_2, ... K_r and update the positions in these dimensions. The update formula is as follows:

$$x_{i,j}^{t+1} = x_{best,j}^{t} + (x_{l,j} + rand \times (x_{u,j} - x_{l,j})) \times \frac{1}{2} \times (\cos(\pi \times \frac{t}{T_{\max}} + 1)), \; j = K_1, K_2, ..., K_{k_r} \tag{13}$$

Here, $x_{i,j}^{t+1}$represents the position of the *t+1*-th individual in the *i*-th dimension when iterating *j*; $x_{best,j}^{t}$ represents the best individual of the entire group in the *t* dimension when iterating *j*. $x_{i,j}$ and $x_{u,j}$ are respectively the upper and lower bounds of the *j*-dimensional search space. *rand* is a random number between 0 and 1.

The structure of the dream optimization algorithm is depicted in Figure 4.

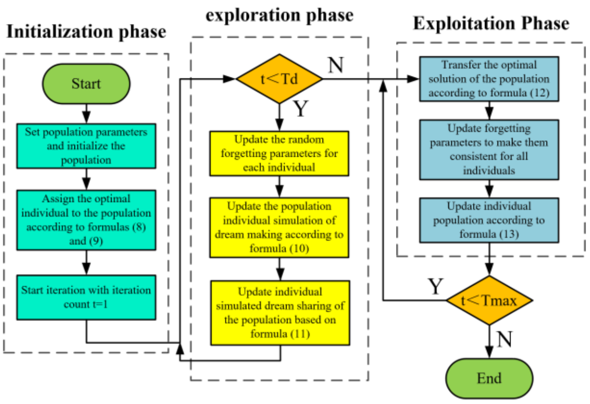

Figure 4: The structure of the dream optimization algorithm

3.5 Improved Dream Optimization Algorithm (IDOA)

The high nonlinearity of lithium-ion battery datasets poses challenges for traditional random search methods in efficiently locating the global optimum within a complex solution space. Consequently, this paper proposes the following enhancements to the DOA algorithm:

(1) Optimal point set initialization scheme

Optimal point set initialization is a method used to generate an initial population. Its distribution is more uniform and diverse than pure random initialization, which can significantly improve the convergence speed and solution quality of the algorithm. Figure 5 shows the schematic diagrams of population initialization for randomly initialized populations and optimal point set initialization.

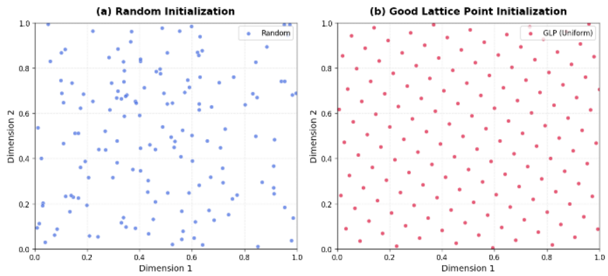

Figure 5: Schematic diagram of population initialization

(2) Adaptive population reduction mechanism

The population reduction mechanism is to gradually reduce the population size during the algorithm's operation based on the search progress or the number of evaluations, thereby gradually focusing computing resources from the initial extensive exploration to the later fine development. Suppose the initial population size is NP^{init} and gradually reduces to the minimum value NP^{min} during the optimization process. The formula followed for reduction is:

$$NP_G = NP^{init} - \frac{(NP^{init} - NP^{\min}) \cdot G}{MAX_G} \tag{14}$$

Here, *G* represents the current number of iterations, and MAX_G represents the maximum number of iterations. This reduction mechanism achieves the global and local exploration of the balanced optimization algorithm by dynamically and linearly adjusting the population density. The introduction of this mechanism not only reduces unnecessary computational overhead in the later stage, but also forms a refined search strategy: maintaining a large population in the early stage of iteration to maintain diversity and prevent premature convergence; In the later stage of iteration, focus on the dominant individuals to improve the accuracy of local optimization. Algorithm-1 explains the proposed IDOA-LSTM approach.

Algorithm 1 IDOA-LSTM Training and Hyperparameter Optimization

Input: Battery dataset *D*, Search space bounds [X_L, X_U], Maximum iterations T_{max}, Exploration phase limit

T_d, Initial population size NP_{init}, Minimum population size NP_{min}.
Output: Best hyperparameters X_{best}, Predicted RUL of battery.
1: **Initialize** D_{clean} and D_{norm} via Hampel filter and Min-Max normalization.
2: Split D_{norm} into training set D_{train} and testing set D_{test}.
3: **Initialize** population *Pop* with Optimal Point Set using NP_{init} and bounds $[X_L, X_U]$.
4: **for** $t = 1, 2, \ldots, T_{max}$ **do**
5: **Update** population size NP_t = Round(NP_{min} + NP_{init} - NP_{min})×(1 - t / T_{max}))
6: Retain the best NP_t individuals in *Pop* based on fitness.
7: **for** each individual X_i in *Pop* **do**
8: Build LSTM model with hyperparameters X_i.
9: Calculate fitness $Fitness_i$ using RMSE on D_{train}.
10: **end for**
11: Update global best X_{best} and group bests $X_{best\text{-}group}$.
12: **if** $t < T_d$ **then**
13: Divide *Pop* into 5 groups based on memory differences (*Fitness*).
14: **for** each individual X_i in *Pop* **do**
15: Execute Forgetting and Supplementing strategy using Eq. (11).
16: Execute Dream Sharing strategy using Eq. (13).
17: **end for**
18: **else**
19: **for** each individual X_i in *Pop* **do**
20: Execute Adaptive population reduction strategy using Eq. (14).
21: **end for**
22: **end if**
23: **end for**
24: Train final LSTM model on D_{train} using global optimal X_{best}.
25: Calculate Predicted-RUL on D_{test}.
26: **Return** X_{best} and Predicted-RUL.

To ensure the reproducibility of the experiments, the network architecture and training configurations of the LSTM model are explicitly defined. The proposed network consists of an input layer, a hidden LSTM layer, and a fully connected linear output layer. The standard hyperbolic tangent (Tanh) function is utilized as the state activation function within the LSTM cells. The network is trained using the Adaptive Moment Estimation (Adam) optimizer, aiming to minimize the Mean Squared Error (MSE) loss function. All other structural parameters, such as the sequence length, are kept constant to ensure a controlled experimental environment.

Instead of relying on empirical manual trial-and-error, four key hyperparameters that significantly impact the model's training efficiency and prediction accuracy are dynamically tuned by the proposed IDOA. These targeted hyperparameters include the initial learning rate, the number of neurons in the hidden layer, the batch size, and the total number of training epochs. Specifically, the continuous search space bound for the learning rate is set from 0.0001 to 0.01. For the discrete parameters, the number of hidden neurons is constrained between 16 and 128, the batch size is bounded from 16 to 128, and the training epochs are optimized within a range of 50 to 200. By autonomously exploring these four critical parameters, the IDOA-LSTM framework effectively captures the highly nonlinear capacity degradation trajectories while striking an optimal balance between computational overhead and prediction precision.

4 Data result analysis

4.1 Evaluation Indicators

The prediction results of the model in this paper are evaluated through Root Mean Square Error (RMSE) and Mean Absolute Error (MAE). The following are two assessment indicators:

The prediction results of the model in this paper are evaluated through Root Mean Square Error (RMSE) and Mean Absolute Error (MAE). The following are two assessment indicators:

$$MAE = \frac{1}{N}\sum_{i=1}^{N}\left|y_i - \tilde{y}_l\right| \tag{15}$$

$$RMSE = \sqrt{\frac{1}{N}\sum_{i=1}^{N}(y_i - \tilde{y}_l)^2} \tag{16}$$

Here, N represents the total number of samples in the dataset to be tested; y_i is the observed value of the battery capacity; $\tilde{y}_l$ is the predicted value of battery capacity. The smaller the RMSE and MAE, the better the prediction results of the model.

4.2 Prediction result analysis

To assess the predictive capability of the IDOA-LSTM model, this study employs LSTM, CPO-LSTM, DOA-LSTM, and IDOA-LSTM to train the datasets independently. The models are trained using four groups of battery models derived from the CALCE battery dataset and the NASA PCoE dataset. For the CALCE dataset, a battery-level leave-one-out cross-validation (LOOCV) protocol was implemented to rigorously evaluate the model's generalization ability. In each fold of the four experimental rounds, one battery was designated as the testing set, while the remaining three batteries were utilized for training. This process was rotated until every battery had been used as a test set. Furthermore, to eliminate the bias from random weight initialization and ensure the reproducibility of results, each fold was independently executed 10 times. The final performance metrics reported in this study represent the average values across these multiple splits and runs. The battery remaining useful life prediction results for CALCE are illustrated in Figure 6, while the evaluation metrics for the various prediction models are summarized in Table 2.

Table 2: Comparison of prediction results

Battery	Model	RMSE	MAE
CS_35	LSTM	0.0484	0.0326
	CPO-LSTM	0.0305	0.0256
	DOA-LSTM	0.0286	0.0232
	IDOA-LSTM	0.0201	0.0181
CS_36	LSTM	0.0523	0.0364
	CPO-LSTM	0.0312	0.0274
	DOA-LSTM	0.0256	0.0205
	IDOA-LSTM	0.0198	0.0174
CS_37	LSTM	0.0462	0.0315
	CPO-LSTM	0.0289	0.0214
	DOA-LSTM	0.0264	0.0217
	IDOA-LSTM	0.0213	0.0163
CS_38	LSTM	0.0612	0.0425
	CPO-LSTM	0.0305	0.0283
	DOA-LSTM	0.0225	0.0192
	IDOA-LSTM	0.0186	0.0154

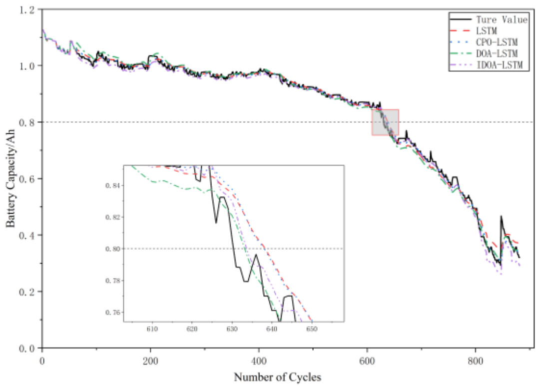

(a) Prediction data of CS_35 battery

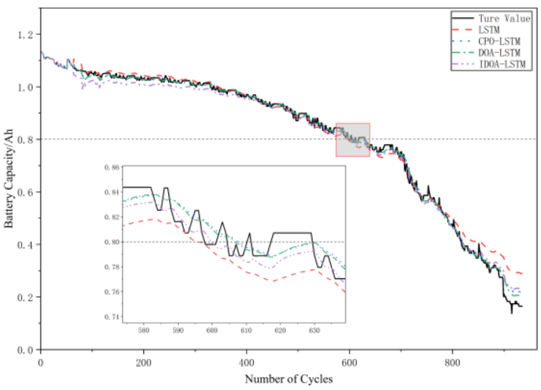

(b) Prediction data of CS_36 battery

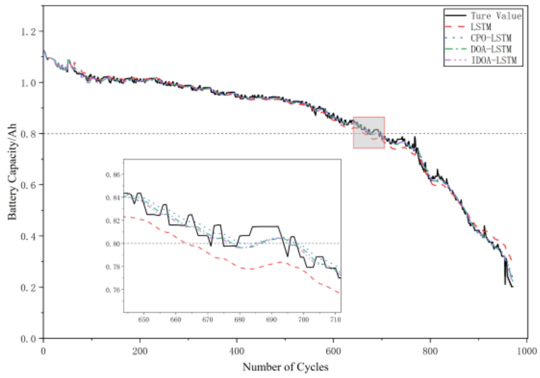

(c) Prediction data of CS_37 battery

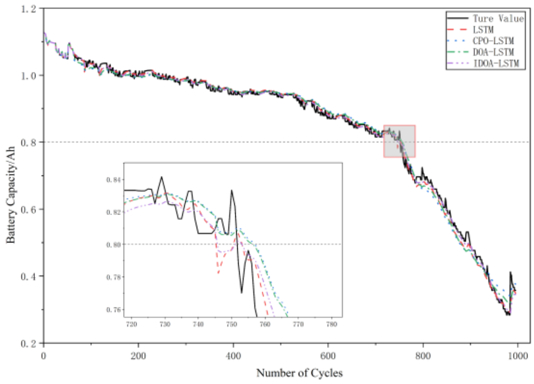

(d) Prediction data of CS_38 battery

Figure 6: Prediction results of different models

The figure demonstrates that the prediction accuracy of the IDOA-LSTM model has improved to varying extents compared to the other models, indicating its superior predictive performance. Furthermore, following enhancements to the IDOA-LSTM model, its predictive accuracy has significantly surpassed that of the DOA-LSTM model. This finding confirms that the modifications made to the IDOA-LSTM method have enhanced the search efficiency of the DOA-LSTM approach and expedited its convergence rate. Additionally, the IDOA-LSTM model is capable of providing more precise predictions of capacity variation amplitudes in specific mutation regions and effectively capturing the majority of degradation trends.

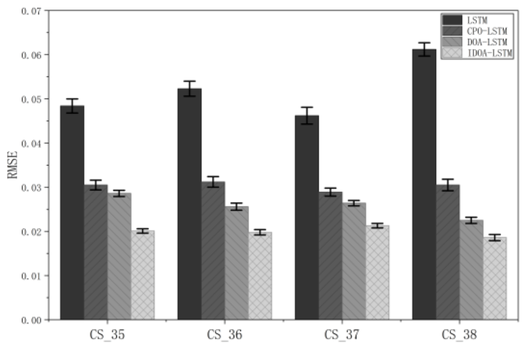

(a) Root mean square error

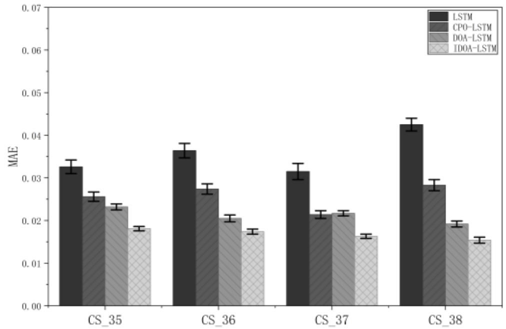

(b) Mean absolute error

Figure 7: Evaluation indicators of different models

To rigorously verify the robustness of the proposed method and rule out the influence of randomness during algorithm initialization, a statistical significance test was conducted. The standard LSTM, DOA-LSTM, and the proposed IDOA-LSTM models were independently executed 10 times using the CS2_35 dataset with different random seeds. As shown in Table 3, the IDOA-LSTM model consistently achieved the lowest Mean RMS, demonstrating exceptional stability with the smallest standard deviation. Furthermore, a paired t-test was performed between the RMSE distributions of the DOA-LSTM and IDOA-LSTM models. The resulting p-value is significantly less than 0.05 ($p<0.001$), mathematically confirming that the performance improvement yielded by the optimal point set and adaptive population reduction mechanisms is statistically significant, rather than a coincidental outcome of random initialization.

Table 3: Statistical Significance analysis over 10 independent runs

Model	Min RMSE	Max RMSE	Mean RMSE
LSTM	0.0461	0.0512	0.0484±0.0016
CPO-LSTM	0.0290	0.0321	0.0305±0.0011
DOA-LSTM	0.0279	0.0301	0.0288±0.0007
IDOA-LSTM	0.0192	0.0210	0.0200±0.0005

To further verify the robustness and universality of the IDOA-LSTM model, the performance of the model is verified using the NASA PCoE dataset below. In this paper, four groups of batteries B0005, B0006, B0007 and B0018 in this dataset are used as the research objects. Its capacity degradation trend shows significant morphological differences from the aforementioned CALCE dataset, which can effectively test the model's extraction ability under different aging characteristics. To address the issue of discontinuous discharge cycle signals in the NASA dataset due to the inclusion of impedance tests, the text uses linear interpolation to fill in the missing capacity nodes and performs serial number re-indexing. Through the above processing, the degradation trajectories of all batteries are uniformly mapped to a continuous time series space, ensuring that the LSTM model can normally perform life prediction. Furthermore, this paper still employs the Leave-one-out cross-validation strategy, taking three sets of batteries as the training set and the remaining one as the test set respectively, in order to evaluate the prediction accuracy of the IDOA-LSTM model on unknown individuals. Table 4 shows the optimal parameters and RMSE of the four groups of battery datasets after optimization. The RMSE result is the mean value after 10 times of operation.

Table 4: Optimal parameters and RMSE of the four groups of battery datasets

Battery	learning rate	neurons	Batchsize	RMSE
B0005	0.00861	67	53	0.0198
B0006	0.00903	63	55	0.0194
B0007	0.00895	65	50	0.0195
B0018	0.0912	69	59	0.0192

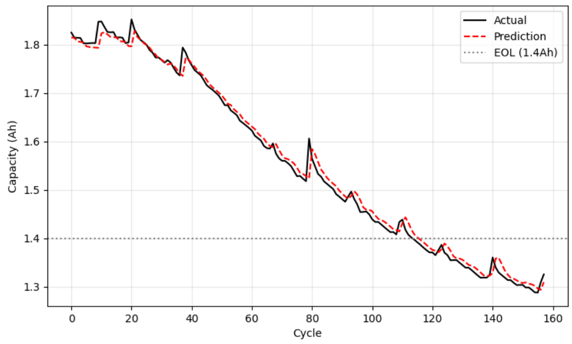

(a) Predicted data of battery B0005

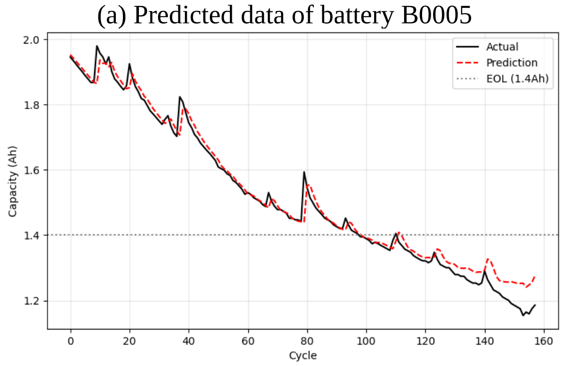

(b) Predicted data of battery B0006

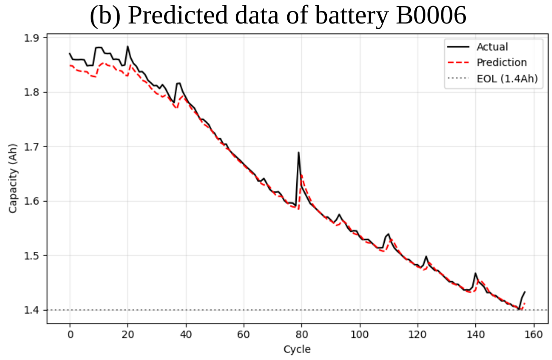

(c) Predicted data of battery B0007

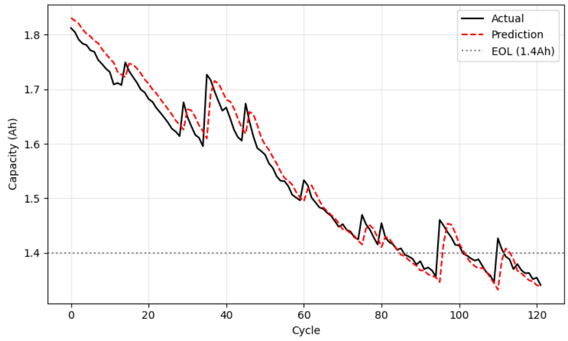

(d) Predicted data of battery B0018

Figure 8: Prediction results of the NASA battery dataset

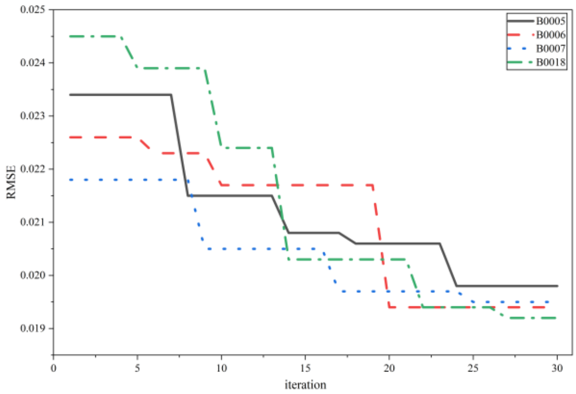

Figure 9: Variation of RMSE error with iteration times

Figure 8 presents the prediction results of the model proposed in this study, utilizing the NASA dataset. The optimized hyperparameters are as follows: the initial learning rate is 0.00861, the number of neurons is 67, and the batch size is 53. Figure 9 illustrates that as the number of iterations of the IDOA algorithm increases, the prediction error, measured by RMSE, gradually decreases, ultimately converging to 0.0192. In comparison to the error prior to optimization, the model error following IDOA optimization is reduced by an average of 21.63%. Furthermore, the potential for additional error reduction remains as the number of iterations increases. Additionally, Figure 9 indicates that the IDOA algorithm achieves a significant reduction in RMSE during the early stages of iteration, which can be attributed to the high-quality population starting point provided by the optimal point set initialization. As iterations progress, the error curve consistently declines in a stepped manner, thereby validating the effectiveness of the adaptive population reduction mechanism in balancing global exploration with local development. These results demonstrate that the IDOA-LSTM model proposed in this study exhibits universality across different models and possesses a degree of robustness, indicating its practical application value.

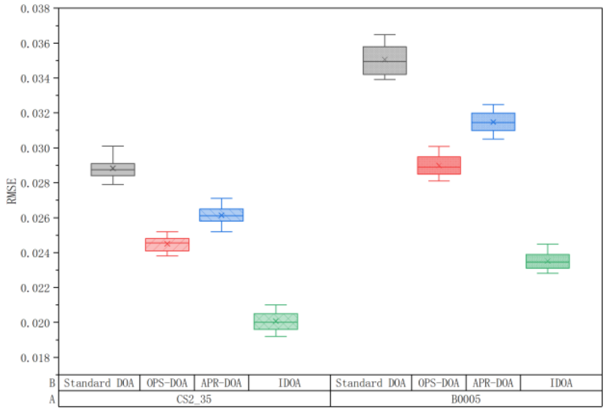

Figure 10: Ablation experiment error box diagrams

Additionally, to validate the individual contributions of the proposed modifications and assess algorithmic robustness, a brief ablation study was conducted. Instead of single-run evaluations, the baseline DOA-LSTM, OPS-DOA-LSTM (only Optimal Point Set), APR-DOA-LSTM (only Adaptive Population Reduction), and the complete IDOA-LSTM were independently executed 10 times with different random seeds on both the CALCE (CS2_35) and NASA (B0005) datasets. The experimental results are shown in Figure 10. The experiments revealed that the baseline DOA-LSTM suffers from relatively high error variance due to random initialization. Incorporating only the Optimal Point Set (OPS) mechanism significantly tightened the variance of the prediction errors, demonstrating enhanced robustness by preventing the algorithm from trapping in local optima. Conversely, employing only the Adaptive Population Reduction (APR) mechanism substantially reduced the overall optimization time by dynamically eliminating redundant individuals. Ultimately, the complete IDOA-LSTM framework achieved the lowest mean error with the narrowest variance. This verifies that the OPS and APR mechanisms are mutually beneficial, rendering the model highly robust against both metaheuristic randomness and varying battery degradation profiles.

Achieving lower RMSE and MAE values in battery RUL prediction is not merely a numerical improvement, but carries profound practical significance for real-world Battery Management Systems . A highly precise RUL prediction effectively narrows the uncertainty margin of the End-of-Life estimation. In practical applications, such as electric vehicles and grid-level energy storage, this precision provides reliable early warning mechanisms to prevent catastrophic failures, such as thermal runaway caused by over-usage. Conversely, it also avoids the economic waste and environmental burden associated with the premature replacement of healthy batteries. Therefore, the significant reduction in prediction error achieved by the proposed IDOA-LSTM model directly translates to enhanced operational safety and economic efficiency.

5 Discuss

In this study, we proposed an IDOA-LSTM model to address the challenges of RUL prediction for lithium-ion batteries. The experimental results, as presented in previous chapters, confirm that the integration of the Improved Dream Optimization Algorithm (IDOA) with the Long Short-Term Memory (LSTM) network significantly enhances predictive performance.

5.1 Interpretation of performance improvements

The superior performance of the proposed model can be attributed to the improvements made to the DOA algorithm. By utilizing an optimal point set for population initialization, the model effectively mitigates the risk of entrapment in local optima, a common limitation in standard metaheuristic-based hyperparameter tuning. Furthermore, the adaptive population reduction mechanism ensures a balance between exploration and exploitation during the optimization process, leading to a faster and more stable convergence compared to traditional LSTM models. These improvements are crucial, as hyperparameter sensitivity is a well-known bottleneck in deep learning-based battery health management.

5.2 Robustness in nonlinear degradation

Unlike model-based approaches that rely heavily on physical parameters—which are often difficult to identify accurately due to internal electrochemical complexity—the data-driven nature of our IDOA-LSTM model allows it to implicitly capture the nonlinear degradation patterns. The results indicate that the IDOA-LSTM model maintains high accuracy even when confronted with diverse charging and discharging conditions. This robustness suggests that the model is well-suited for practical application in Battery Management Systems (BMS) where battery behavior is influenced by complex environmental and operational stressors.

5.3 Comparison with state-of-the-art and novelty statement

Compared to the existing state-of-the-art approaches summarized in Table 1 and the comparative baselines in Table 2, the proposed IDOA-LSTM framework demonstrates superior predictive accuracy and algorithmic robustness. While numerous existing studies have employed metaheuristic algorithms to optimize LSTM networks, a persistent limitation in these approaches is the imbalance between global exploration and local exploitation, often resulting in entrapment in local optima and high computational overhead when processing highly nonlinear battery degradation data. The fundamental novelty of our IDOA-LSTM lies in overcoming these specific bottlenecks. By seamlessly integrating the Optimal Point Set (OPS) for high-quality, uniform initialization and an Adaptive Population Reduction (APR) mechanism for dynamic computing resource allocation, our framework fundamentally enhances the hyperparameter search efficiency. Consequently, as evidenced by the results, the IDOA-LSTM effectively captures complex degradation trajectories—including the severe capacity regeneration phenomena in the NASA dataset—yielding the lowest RMSE and MAE compared to traditional optimization-enhanced models.

5.4 Limitations and future perspectives

Despite the high accuracy achieved, this study has certain limitations. First, the model's performance relies on the quality and quantity of historical training data. In scenarios where battery aging data is extremely scarce or characterized by unexpected health indicators, the predictive accuracy might fluctuate. Second, while the IDOA-LSTM model demonstrates improved convergence, the computational cost of the optimization process during training remains an aspect to consider for real-time onboard deployment.

Future work will focus on two directions: (1) integrating transfer learning to enhance model adaptability across different types of batteries with minimal training samples; and (2) implementing a more lightweight version of the optimized model to facilitate seamless integration into low-power embedded BMS environments.

6 Conclusion

To achieve accurate prediction of RUL for lithium-ion batteries, this paper proposes a RUL prediction model based on IDOA-LSTM. For the health indicators extracted from the charging and discharging process, Hampel filtering is used to remove outliers in the indicator data and normalize the data. Secondly, when using the LSTM model for prediction, in order to find the best LSTM hyperparameters more quickly and accurately, some improvements are made to the traditional DOA to enhance its optimization ability. The simulation results of the four battery datasets of the CS2 series show that the prediction accuracy of the IDOA-LSTM model is higher than that of other models. Moreover, compared with the results of other existing prediction models, this model still has superior performance. The prediction results of the NASA battery dataset show that this model has certain universality and robustness and can adapt to different battery datasets for remaining life prediction.

Despite the promising performance of the IDOA-LSTM model, several limitations warrant further discussion. First, the model's performance was validated primarily on specific datasets, which raises concerns regarding its generalization across different battery chemistries. Since electrochemical degradation mechanisms vary significantly between chemistries, the model’s transferability without extensive retraining remains to be rigorously tested. Second, while IDOA effectively optimizes hyperparameters, the model’s predictive accuracy remains sensitive to structural configurations, such as sequence length and the number of layers, posing a risk of overfitting on specific datasets. Finally, the computational overhead inherent in the iterative IDOA process presents practical challenges for real-time deployment on resource-constrained embedded Battery Management Systems. Addressing these challenges, future research will focus on integrating transfer learning techniques to enhance cross-domain adaptability with minimal historical data, exploring model compression and pruning strategies to facilitate lightweight onboard deployment, and incorporating probabilistic forecasting to quantify prediction uncertainty, thereby providing a more reliable decision-making basis for safety-critical applications.

The CALCE and NASA battery degradation datasets analyzed in this study are publicly available. The original IDOA-LSTM implementation code and the pre-processed data supporting the findings of this study are available from the corresponding author upon reasonable request.

References

[1] Xiaoxue W, Yupeng H, Yixin L, et al (2026). Deep Reinforcement Learning-based Coordinated Optimization Between Distribution Networks and Microgrids Towards Demand Response Uncertainty. *Energy and AI*. DOI: 10.1016/j.egyai.2026.100717.

[2] Zhu Zhenyu (2022). Life Cycle Assessment of Lithium-ion Batteries Oriented to the "Dual Carbon" Strategic Goals: Framework, Methods and Progress. *Journal of Mechanical Engineering*. DOI: 10.3901/JME.2022.22.003.

[3] Liu, Y. Wang, L. Li, D. et al (2023). State-of-health estimation of lithium-ion batteries based on electrochemical impedance spectroscopy: a review. *Protection And Control Of Modern Power Systems*. DOI: 10.1186/s41601-023-00314-w.

[4] Guolian Hou, Fan Zhang, Congzhi Huang, Ting Huang (2025). Joint prediction of SOH and RUL for Lithium-ion batteries by an enhanced Transformer model with physical information constraints. *Energy*. DOI: 10.1016/j.energy.2025.138435.

[5] Jie Li, Shiming Zhao, Md Sipon Miah, Mingbo Niu (2023). Remaining useful life prediction of lithium-ion batteries via an EIS based deep learning approach. *Energy Reports*. DOI: 10.1016/j.egyr.2023.10.030.

[6] Xin Li, Yan Ma, Jiajun Zhu (2021). An online dual filters RUL prediction method of lithium-ion battery based on unscented particle filter and least squares support vector machine. *Measurement*. DOI: 10.1016/j.measurement.2021.109935.

[7] Isaiah Oyewole, Youngki Kim, Abdallah Chehade (2025). A conditional mixture model with recurrent neural network for prognostic analysis of lithium-ion batteries. *Journal of Energy Storage*. DOI: 10.1109/ecce58356.2025.11260161.

[8] Zhuqing Wang, Ning Liu, Chilian Chen, Yangming Guo (2023). Adaptive self-attention LSTM for RUL prediction of lithium-ion batteries. *Information Sciences*. DOI: 10.1016/j.ins.2023.01.100.

[9] A. Tomar, M. Gupta, J. Mittal, A. Arya and U. Varshney (2025). Prediction of SOH and RUL for Li-Ion Batteries in EV Based on AttentiveLSTM Multi-Task Model. *Emerging and Selected Topics in Industrial Electronics*. DOI: 10.1109/JESTIE.2025.3576185.

[10] L. Li, Z. Huang and G. Ding. Indirect Prediction for Lithium-Ion Batteries RUL Using Multi-Objective Arithmetic Optimization Algorithm-Based Deep Extreme Learning Machine. *IEEE Access*. DOI: 10.1109/ACCESS.2023.3320058.

[11] M. Zhu, Q. Ouyang, Y. Wan and Z. Wang (2023). Remaining Useful Life Prediction of Lithium-Ion Batteries: A Hybrid Approach of Grey–Markov Chain Model and Improved Gaussian Process. *Emerging and Selected Topics in Power Electronics*. DOI: 10.1109/JESTPE.2021.3098378.

[12] T. Jing et al (2025). A Hybrid Data-Driven Granular Model for Battery Remaining Useful Life Prediction. *IEEE Transactions on Instrumentation and Measurement*. DOI: 10.1109/TIM.2025.3541804.

[13] G. Ye, L. Feng, J. Guo, Y. Chen and S. Li (2025). A Simple and Effective KAN-Based Architecture for Accurate Battery RUL Prediction. *IEEE Access*. DOI: 10.1109/ACCESS.2025.3590480.

[14] Z. Bao, T. Luo, M. Gao, Z. He, K. Gao and J. Nie (2025). A Lightweight and Term-Arbitrary Memory Network for Remaining Useful Life Prediction of Li-Ion Battery. *IEEE Transactions on Instrumentation and Measurement*. DOI:10.1109/TIM.2025.3556835.

[15] J. Zhang et al (2024). A Data-Model Interactive Remaining Useful Life Prediction Approach of Lithium-Ion Batteries Based on PF-BiGRU-TSAM. *IEEE Transactions on Industrial Informatics*. DOI: 10.1109/TII.2023.3266403.

[16] L. Li, Y. Li, R. Mao, L. Li, W. Hua and J. Zhang (2023). Remaining Useful Life Prediction for Lithium-Ion Batteries With a Hybrid Model Based on TCN-GRU-DNN and Dual Attention Mechanism. *IEEE Transactions on Transportation Electrification*. DOI: 10.1109/TTE.2023.3247614.

[17] Yifan Lang, Yuelin Gao (2025). Dream Optimization Algorithm (DOA): A novel metaheuristic optimization algorithm inspired by human dreams and its applications to real-world engineering problems. *Computer Methods in Applied Mechanics and Engineering*. DOI: 10.1016/j.cma.2024.117718.